Agència de Gestió d'Ajuts Universitaris i de Recerca

Memòria justificativa de recerca de les convocatòries BCC, BE, BP, CTP-AIRE, DEBEQ, FI, FI-ICIP, INEFC i PIV

La memòria justificativa consta de les dues parts que venen a continuació:
1.- Dades bàsiques i resums
2.- Memòria del treball (informe científic)

Tots els camps són obligatoris

1.- Dades bàsiques i resums

Nom de la convocatòria

BP

Llegenda per a les convocatòries:

BCC	Convocatòria de beques per a joves membres de comunitats catalanes a l'exterior
BDH	Beques i ajuts postdoctorals del Programa DGR-Henkel KGaA
BE	Beques per a estades per a la recerca fora de Catalunya
BP	Convocatòria d'ajuts postdoctorals dins del programa Beatriu de Pinós
CTP-AIRE	Ajuts per accions de cooperació en el marc de la comunitat de treball dels Pirineus. Ajuts de mobilitat de personal investigador.
DEBEQ (Modalitat A3)	Beques de Cooperació Internacional i Desenvolupament
FI	Beques predoctorals per a la formació de personal investigador
FI-ICIP	Beques i ajuts per a l'etapa de formació i de recerca de personal investigador novell en els àmbits d'interès de l'Institut Català Internacional per la Pau
INEFC	Beques predoctorals i de col·laboració, dins de l'àmbit de l'educació física i l'esport i les ciències aplicades a l'esport
PIV	Beques de recerca per a professors i investigadors visitants a Catalunya

Títol del projecte: ha de sintetitzar la temàtica científica del vostre document.
Síntesi i propietats de vidres metàl·lics massissos i materials nanocomposites basats en Fe per aplicacions com a materials magnètics tous.

Dades de l'investigador o beneficiari

Nom	Cognoms
Joan	Torrens Serra

Correu electrònic
j.torrens@uib.es

Dades del centre d'origen

Institut für Komplexe Materialien, Leibniz-Institut für Festkörper- und Werkstoffforschung Dresden.

Número d'expedient

2009 BPA 00138

Paraules clau: cal que esmenteu cinc conceptes que defineixin el contingut de la vostra memòria.
Cinètica de cristal·lització, vidres metàl·lics, materials magnètics tous, efecte magnetocalòric, cristal·lització

Data de presentació de la justificació

10/01/2012

Nom i cognoms i signatura del/de la investigador/a	Vist i plau del/de la responsable de la sol·licitud

Resum del projecte: cal adjuntar dos resums del document, l'un en anglès i l'altre en la llengua del document, on s'esmenti la durada de l'acció

Resum en la llengua del projecte (màxim 300 paraules)
En aquest projecte, realitzat del 1 de desembre del 2010 fins el 31 de desembre del 2011, s'ha explorat l'efecte de les condicions i influència dels elements d'aleació en la capacitat de formació de vidre, l'estructura i les propietats tèrmiques i magnètiques de vidres metàl·lics massissos i materials nanocristal·lins en base Fe. La producció d'aquests materials en forma de cintes de unes 20 micres de gruix ha estat àmpliament estudiada i s'ha vist que presenten unes propietats excel·lents com a materials magnètics tous. El propòsit general d'aquest projecte era l'obtenció de composicions òptimes amb alta capacitat de formar vidre i amb excel·lents propietats magnètiques com a materials magnètics tous combinat amb bones propietats mecàniques. El projecte prenia com a punt de partida l'aliatge [FeCoBSi]96Nb4 ja que és el que presenta millor capacitat de formar vidre i presenta una alta imantació de saturació i baix camp coercitiu. S'ha fet un estudi dels factors fonamentals que intervenen en la formació de l'estat vitri. La composició abans esmentada ha estat variada amb l'addició d'altres elements per estudiar com afecten aquests nous elements a les propietats, la formació de vidre i l'estructura dels aliatges resultants amb l'objectiu de millorar-ne les propietats magnètiques i la capacitat de formació de vidre. Entre altres s'ha usat el Zr, Mo, Y i el Gd per millorar la formació de vidre; i el Co i el Ni per millorar les propietats magnètiques a alta temperatura.
S'han estudiat les relacions entre la capacitat de formació de vidre i la seva estabilitat tèrmica, la resistència a la cristal·lització i la estructura de l'aliatge resultant després del procés de solidificació. Per aquest estudi s'han determinat els mecanismes que controlen la transformació i la seva cinètica així com les fases que es formen durant el tractament tèrmic permetent la formulació de models predictius.

Resum en anglès (màxim 300 paraules)
This project, conducted from 1 December 2010 until 31 December 2011, has explored the effect of conditions and the influence of alloying elements on the glass forming ability, structure, thermal and magnetic properties of metallic glasses and nanocrystalline Fe-based alloys. The production of these materials in the form of ribbons about 20 microns thick has been widely studied and has shown some excellent properties as soft magnetic materials. The purpose of this project was to obtain optimum compositions with high glass forming ability and excellent magnetic properties as soft magnetic materials combined with good mechanical properties. The project took as its starting point the alloy [FeCoBSi] 96Nb4 which presented very good ability to form glass and has a high saturation magnetization and low coercive field. The above composition was varied with addition of other elements to study how these affect the properties, the glass formation and structure of the resulting alloys with the aim of improving the magnetic properties and ability of glass formation. Among others Zr, Mo, Y and Gd were used to enhance the formation of glass, and the Co and Ni to improve the magnetic properties at high temperature.
We have studied the relationship between the glass forming ability and thermal stability, resistance to crystallization and structure of the alloy resulting from the solidification process. For this study we have determined the mechanisms that control the transformation and

Resum en anglès (màxim 300 paraules) – continuació -.

its kinetics and the phases formed during heat treatment allowing the formulation of predictive models.

2.- Memòria del treball (informe científic sense limitació de paraules). Pot incloure altres fitxers de qualsevol mena, no més grans de 10 MB cadascun d'ells.

1. The thermal stability, crystallization and magnetic properties of $[(Fe,Co)_{0.75}Si_{0.05}B_{0.20}]_{96-y}Nb_4X_y$ bulk metallic glasses

This section corresponds to the Goal 1,2 of the original project presented in the application for the grant.

In the last decade great efforts have been done to overcome the size limitation imposed by the high cooling rates needed in the production of bulk metallic glasses. Bulk glassy multicomponent alloys with different compositions have been achieved as rods of several cms [1]. In the case of Fe-based bulk metallic glasses, different families of alloys have been successfully developed. Among them, (Fe,Co)-B-Si-Nb presents high glass forming ability (up to 5 mm) and good functional properties as excellent soft magnetic characteristics (M_s~1T, μ~12000 and H_c~2 A/m) combined with high fracture strength (σ_f~4000 MPa) and high corrosion resistance [2]. Extended investigation on the role that play the different alloying elements has leaded to a optimal composition $[(Fe,Co)_{0.75}Si_{0.05}B_{0.20}]Nb_4$ with the best Fe/Co ratio between 60/40 and 50/50. The addition of Co not only enhances glass forming ability due to a larger negative mixing enthalpy with Nb than Fe, but also produces an increase in the saturation polarization and Curie temperature because of the stronger exchange coupling between Fe-Co atoms [3]. Recently, different studies have been devoted to improve this alloy. An enhancement of ductile strain is obtained by replacing Co by Ni but reduces Young modulus and fracture strength [4]. The origin of the good glass forming ability in this kind of alloys seems to be related with the primary crystallization of a complex $Fe_{23}B_6$ phase in contrast to the NANOPERM type alloys with bcc-Fe phase. However, only few studies have been done concerning the crystallization kinetics.

1.1 Influence of alloying elements on the glass forming ability and thermal stability

First of all the influence of the substitution of some transition metals and rear earths were investigated. The master alloys of $[(Fe_{60}Co_{40})_{0.75}Si_{0.05}B_{0.20}]_{96-x}Nb_4M_x$, (M=Zr, Mo, Y, Gd; x=0,1,2) compositions,

from now on designed as $A_{96-x}Nb_4M_x$, were prepared in several steps, using arc melting in a Ti-gettered high purity Ar atmosphere. First of all, eutectic 25Fe75Nb (wt.%) and 24Fe76Nb (wt.%) prealloys were produced by melting pure Fe (99.9 mass %), Y and Nb (99.9 mass %) lumps. Further, proper quantities of FeNb and FeY prealloy, together with the rest of necessary Fe, Ni, Co lumps (99.9 mass %), crystalline B (99 mass %), and Si lumps (99.99 mass %), Mo and Gd were melted together. The as-melted buttons were re-melted several times in order to assure a good homogeneity of the entire master alloy.
Ribbons with a thickness of 20-30 μm and a width of 3-4 mm were prepared by single-roller melt spinning at a linear speed of 40 m/s. Pieces of each master alloy were re-melted in quartz tubes and then the melt injected into a water-cooled copper mold in a high-purity argon atmosphere to produce rod-shaped specimens with different diameters.
For the original alloy (x=0), the proper casting temperature has been determined to be in the range of 1275 and 1300 °C. This is about 100°C above the melting temperature determined by differential scanning calorimetry (DSC).

The X-ray diffraction patterns of as-quenched ribbons are presented in figure 1. All the melt spun ribbons show a disordered type pattern with broad diffraction peaks and the absence of crystalline peaks. In order to study the differences between the compositions, the amorphous structure has been inspected using high resolution Synchrotron XRD at P07 (Physics hutch) beamline of PETRA III storage ring (Hamburg, Germany). Samples were measured in transmisison geometry. The wavelength was 0.01548 nm (E=80.09 keV). The beam size was set to 0.5x0.5 mm^2. Samples were illuminated for 25 s. The two main broad peaks of have been fitted by a Gaussian function in order to determine the peak position The highest value is found for the $A_{96}Nb_4$ alloy, while lower values are obtained for alloys with x=2. As the units of peak position (q) are given in $Å^{-1}$, its inverse (1/q) is directly related to the distance between atoms. Then, lower values of *q* are related with closer packed structures.

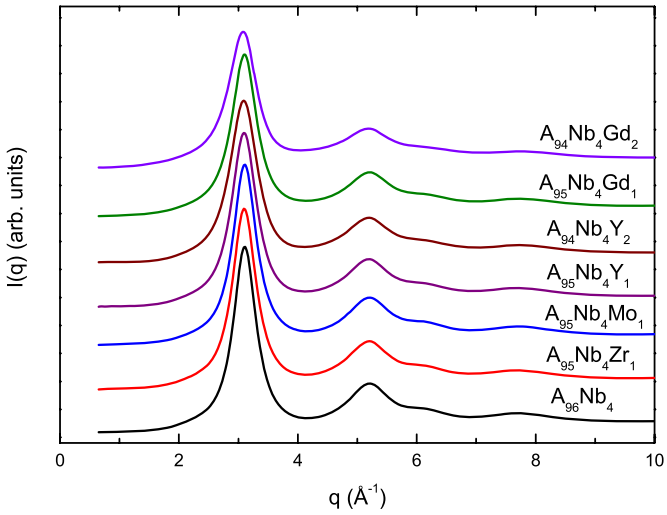

Fig 1. Synchrotron XRD patterns for the as-quenched ribbons

In order to study the ability of these alloys to be produced in bulk glasses, rods of diameters (d) from 1.5 to 2.5 mm were prepared for all compositions by injection casting. For all compositions, except for $A_{95}Nb_4Gd_1$ one, rods of d=1.5 mm have been obtained in fully amorphous state, as shown in the XRD patterns (Fig. 2). However, amorphous d=2 mm rods were only obtained for $A_{95}Nb_4Zr_1$ and $A_{95}Nb_4Mo_1$ alloys.

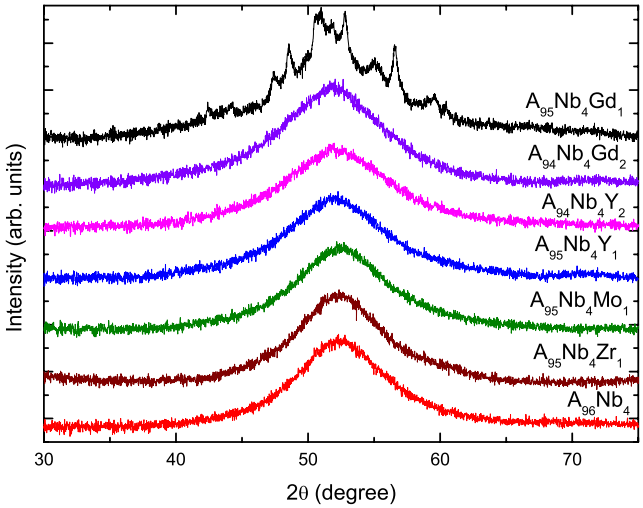

Fig 2. XRD patterns for the as-casted 1.5 mm rods.

The thermal stability of the samples has been studied by differential scanning calorimetry. The thermal stability and the melting behavior of the glassy samples were evaluated using a NETZSCH DSC 404 differential scanning calorimeter (DSC) at a heating rate of 20 K/min under a flow of high purity argon. The temperature values have been obtained as a mean value of different measurements. The standard deviation is within ±1 K. All the alloys exhibit an endothermic event, characteristic of the glass transition, previous to the first exothermic peak. The crystallization proceeds in two (for Y containing alloys) or three different (other ones) stages in these alloys. At higher temperatures endothermic peaks corresponding to the melting of the alloy are observed. The addition of Zr, Gd and Y leads to an increase in both the glass transition temperature and the onset temperature of the primary crystallization in respect to the M-free alloy while the effect of Mo is to slightly decrease both temperatures. However, the Y and Gd leads to the highest enhancement of the thermal stability and to a wider supercooled liquid range (SLR), from ΔT_x=41 for $A_{96}Nb_4$ to about $\Delta T_x \approx 56$ for Gd and Y-containing alloys. Different criteria have been used in literature to elucidate the GFA. The most direct one is the extension of the supercooled range. The higher ΔT_x the lower tendency of the alloy to crystallize. In the case of our alloys, a better GFA would be found for Y and Gd alloys which have about 16 K larger SLR than others. Another popular criterion is the Turnbull's criterion [5], $T_{gr}=T_g/T_l$. Our results indicate that $A_{95}Nb_4Zr_1$ alloy would have the best GFA whereas using the Liu or γ criterium [6], with $\gamma = \frac{T_x}{T_g + T_l}$, $A_{95}Nb_4Y_1$ and $A_{94}Nb_4Y_2$ alloys are the best among them. As the use of different criteria lead to different results we may compare them to direct experimental results on the critical diameter of casted rods. Only two alloys could be casted with a diameter of 2 mm, $A_{95}Nb_4Zr_1$ and $A_{95}Nb_4Mo_1$. The minor elements added also accomplish the empirical rules of a large mismatch in the atomic radii and negative mixing enthalpies [1]. Gd and Y have larger atomic radii (180 pm) than Zr (155 pm) and Mo (145 pm) [7] but Zr has the largest mixing enthalpies with Fe (-25 kJ/mol), Co (-41 kJ/mol), B (-71 kJ/mol) and Si (-84 kJ/mol) whereas Mo has the lowest with Co (-5 kJ/mol), B (-34 kJ/mol) and Si (-35 kJ/mol). No data has been found for Gd-Si and Y-Si, but with the values of B-Y (-50 kJ/mol) and B-Gd (-50 kJ/mol), one may expect similar values for Si. Clearly, the thermodynamic criteria do not agree with the casting results, except for the case of $A_{95}Nb_4Zr_1$ where a good GFA is predicted from Turnbull's criterion and the large negative mixing enthalpy rule. However, the influence of casting conditions can not be ruled out.

In order to study the influence of replacement of Co by Ni, the highest glass forming alloy, $A_{95}Nb_4Zr_1$, has been chosen. The alloys $[(Fe_{60}Co_{40-x}Ni_x)_{0.75}Si_{0.05}B_{0.20}]_{95}Nb_4Zr_1$ with (x=0,10) (from now on the alloys will be designed as Ni0 and Ni10). The procedure followed in this investigation is the same as in the other alloys. Ribbons have been obtained using melt spinning technique. Also rods of diameters from 1.5 to 2.5 mm have been obtained by direct injection casting. The XRD for the ribbons show the typical diffuse halo for disordered structures indicating that are fully amorphous. In the case of the rods, the XRD experiments indicate that rods of Ni10 alloy have been obtained in fully amorphous state only could be obtained up to 1.5 mm in comparison to Ni0 which was obtained up to 2 mm.
Comparing the calorimetric curves obtained at 20 K/min, both alloys present a clear change in the heat capacity (C_p) corresponding to the glass transition previous to the first exothermic peak. The glass transition temperature (T_g) shifts from the 825±2 K to 814±1 K with the addition of Ni. But the supercooled liquid region, increases from 41 K to 62 K with Ni, indicating a better glass forming ability. Using the Turnbull criterium [5], T_{gr}=0.591 for Ni0 alloy and T_{gr}=0.580 for Ni10 alloy whereas the Liu or γ criterium [6] gives a larger value (γ=0.395) for Ni10 alloy than for Ni0 alloy (γ=0.390). The first crystallization starts a very sharp beginning but tends to smooth at last stages. Its onset temperature increases about 10 K by the addition of Ni as shown in Table 1. The values of primary crystallization enthalpy (ΔH) are very similar in both cases what indicates a very similar transformed value. After the first exothermic peak two more crystallization stages are found. However they present significative differences. The second peak is shifted to lower temperatures with Ni addition and become more extended in temperature and with a lower value of the crystallization enthalpy. The third peak also shows a reduction in the peak temperature with Ni addition but presents a more exothermic event than in the Ni free ribbon. Both melting events show a multiple-peaks fusion indicating that these compositions are far from the eutectic point. However, the melting interval, $\Delta T_M=T_l-T_m$, is expanded by the addition of Ni, from 83 K to 91 K.

The DSC scans after subtracting the ΔC_p contribution for the as-casted rods of Ni0 alloy are compared to the ribbon in figure 3. No difference in the temperatures of glass transition and only a shift of 2 K in the crystallization onset is observed in respect to the ribbon. The value of crystallization enthalpy, ΔH, for the 1.5 mm and 2 mm rods are 34 J/g and 36 J/g, respectively. These values are very similar to that of the ribbon 35 J/g, within the experimental uncertainity which indicates a fully amorphous rod. However, a significant reduction of enthalpy, about 25 %, is observed in the 2.5 mm rod (27 J/g) corresponding to the reduction in the primary transformed fraction due to the quenched-in crystallites during casting.

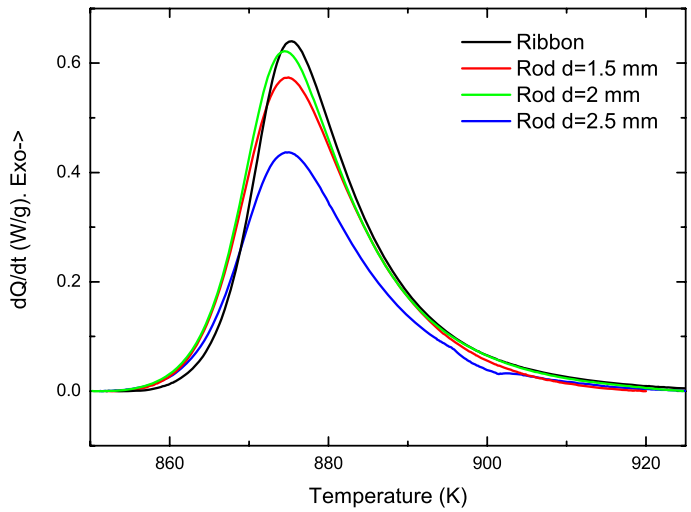

Fig 3. DSC scans of the first peak for the as-casted ribbons and rods.

The replacement of Co by Ni has an important effect over the glass forming ability. The supercooled liquid region is expanded and the glass is more stable against crystallization in accordance with the maximization of the γ parameter although the Turnbull criterium gives a contradictory result which is explained by the larger melting temperature range. The change in the glass forming ability may be related to the larger absolute value the mixing enthalpies of Ni with Zr and Nb (-49 and -30 kJ/mol) than Co (-41 and -25) [7]. The atomic radii of Co and Ni are very similar (124 and 126 pm) so no changes in the glassy structure are expected. However, no fully amorphous rods of Ni10 alloy could be quenched above 2 mm of diameter. It has to be said that Shen [4] reported rods of the same composition up to 6 mm.

1.2 Influence of alloying elements on the microstructural evolution during heating

The changes in the microstructure and the phase evolution after different crystallization events were studied by means of XRD. Samples of ribbons of both alloys have been heated up to temperatures corresponding to the completion of different crystallization events.
The density measurements of the 1.5 mm diameter rods indicate a decrease with Ni from ρ=7.576 g/cm^3 for Ni0 to ρ=7.543 g/cm^3 for Ni10 which may be explained by the lower atomic weight of Ni compared to Co and/or a more compact packing of the amorphous phase. After nanocrystallization, the density for both alloys increases to ρ=7.633 g/cm^3 and ρ=7.595 g/cm^3 for Ni0 and Ni10 respectively. The density value of nanocrystallized Ni0 alloy is similar to that obtained for the 2.5mm diameter rod (ρ=7.646 g/cm^3) of the same alloy which show partially crystallization upon casting.
The changes in the microstructure and the phase evolution after different crystallization events were studied by means of XRD. Samples of ribbons of both alloys have been heated up to temperatures corresponding to the completion of different crystallization events. After the first crystallization peak the precipitation of the metastable $Fe_{23}B_6$ phase is observed in both alloys. This phase is commonly found in high boron content Fe-based metallic glasses and was also observed in similar compositions [3,4,8]. In further crystallization events, the already crystallized boride phase develops and the other phases as bcc-Fe, Fe_2B and Fe_3Si precipitate. In orther to obtaine more detailed information about the crystallization process the alloys are currently studied by Transmission Mössbauer spectroscopy in collaboration with Dr. Pere Bruna from the Universitat Politècnica de Catalunya. The investigations are not completed at this moment but will finish during the next months.

1.3 Influence of alloying elements on the magnetic properties of glassy and nanocrystalline alloys

The influence of alloying in the magnetic properties was investigated for both amorphous and nanocrystalline alloys using the conventional techniques. The M(H) loops have been obtained using vibrating sample magnetometry (VSM) at room temperature. The M(H) curves for some as-quenched and nanocrystallized ribbons (heated up to the end of the first crystallization event) are presented in Figure 4.

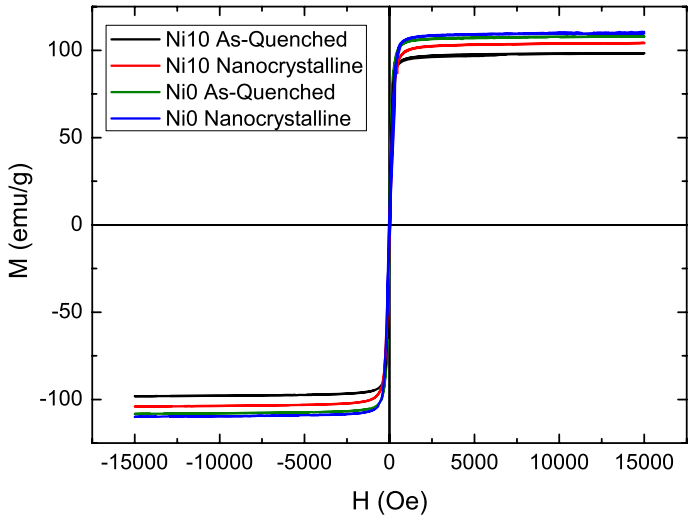

Figure 4. M(H) curves for as-quenched and nanocrystalline ribbons Ni0 and Ni10 alloys.

They display the typical behaviour for a soft magnetic ferromagnet. Also, the saturation polarization (J_s) was calculated from the density measurements using:

$$J_s = 4\pi 10^{-4} M_s \rho \quad (1)$$

with M_s in emu/g. The Curie temperatures of the amorphous phase and nanocrystallized material have been calculated from the thermomagnetic curves using Herzer method [9]. The coercivity has been measured using a Foersters koerzimat.

Let's analyse the influence of the different alloying elements. The $A_{96}Nb_4$ alloy show the highest saturation polarization for both amorphous and nanocrystalline states. The addition of the alloying elements decreases saturation magnetization as can be observed in the table.

Alloy	T_{cA} (K)	$T_{ca'}$ (K)	H_{cA} (A/m)	M_{sA} (emu/g)	J_A (T)	M_{sN} (emu/g)	J_N (T)
$A_{96}Nb_4$	676±1	724±2	2.2±1.1	113±1	1.08±0.01	117±3	1.11±0.02
$A_{95}Nb_4Zr_1$	658±1	733±2	5.3±1.1	109±1	1.04±0.01	111±1	1.06±0.01
$A_{95}Nb_4Mo_1$	660±1	701±2	2.3±0.5	110±1	1.05±0.01	113±2	1.08±0.02
$A_{95}Nb_4Y_1$	622±2	708±4	6.2±1.2	105±2	0.99±0.02	106±2	1.00±0.01
$A_{94}Nb_4Y_2$	625±1	723±2	9.3±0.7	106±2	1.00±0.02	106±2	1.00±0.01
$A_{95}Nb_4Gd_1$	666±1	730±2	10.7±0.5	108±1	1.04±0.01	110±1	1.06±0.01
$A_{94}Nb_4Gd_2$	624±3	726±5	3.6±1.3	96±2	0.93±0.02	100±2	0.96±0.02
Ni10	593±1	726±3	3.2±0.6	97±2	0.92±0.02	103±2	0.98±0.02

In the case of the Ni substituted alloy, the saturation polarization decreases with the addition of Ni in both glassy and nanocrystalline ribbons. The values are comparable to those obtained by Stoica [9] in similar alloys.
Let's compare the magnetic properties of the ribbons with the rods in Ni0 alloy. The measurements in the rods lead to values for the three diameters in Ni0 rods M_s=109±1 emu/g, M_s=109±1 emu/g and M_s=110±2 emu/g for d=1.5, 2 and 2.5 mm respectively. The results for the amorphous rods coincide with values for the amorphous ribbons, in the uncertainty range, and those for the partially crystalline rods correspond with the nanocrystalline ribbons. In the case of Ni0, the low difference between amorphous and nanocrystalline values is also observed in the thermomagnetic curves obtained using a Faraday Thermomagnetic balance.
The as-quenched ribbons present the typical values of coercivity of good soft magnetic materials, presenting in most of the cases coercivity values below 10 A/m. However, two alloys ($A_{95}Nb_4Gd_1$ and $A_{94}Nb_4Y_2$) present larger values than the other compositions. In alloy Ni10 the coercivity of samples annealed up to 773 K and 858 K gives 4.1±0.2 and 4.8±0.1 respectively indicating no relaxation recovery and no significant increase before reaching the onset temperature of crystallization. After the first crystallization the sample maintain low values, H_{cr923}=13.9±0.9 A/m for Ni0 and H_{cr923}=21.3±0.2 for Ni10. After secondary crystallization, the coercivity of both alloys increases drastically to H_{cr983}=211±3 A/m and 266±1 A/m for Ni10 and Ni0 respectively. The coercivity of the rods of Ni0 alloy grow from 2.1±0.1 A/m for d=1.5 mm to 693±5 A/m obtained in the partially crystalline rod with a diameter d=2.5 mm.
The amorphous alloys both in ribbon and rod form are excellent soft magnetic materials with coercivities below 5 A/m. In absence of crystallinity, the main contribution to magnetic anisotropy may be the stress introduced during the quenching which pins the domain wall movement. However, we couldn't observe a reduction after annealing. The precipitation of the nanocrystalline boride leads to an increase of the coercivity but the values still low due to the small size of the nanocrystals as explained in the Herzer's random anisotropy model. Further precipitation at second crystallization increases the grain size and subsequently the magnetocrystalline anisotropy. The same effect is observed in the partially crystalline.

Output of the research results.

The results obtained in this section are expected to be published in high impact peer reviewd journals. Two manuscripts are currently under preparation to be submitted in the following months.

The results may be presented in international conferences during 2012 such as IWNCS 2012 or ISMANAM 2012.

References

[1] A. Inoue, A. Takeuchi, Acta Mater. 59 (2011) 2243-2267.
[2] A. Inoue, B.L. Shen, C.T. Chang, Acta Mater. 52 (2004) 4093-4099
[3] R. Li, S. Kumar, M. Stoica, S. Roth, J. Eckert, J. Phys. D: Appl. Phys. 42 (2009) 085006.
[4] B. Shen, C. Chang, A. Inoue, Intermetallics 15 (2007) 9-16; C. Chang, B. Shen, A. Inoue, Mat. Sci. Eng. A 449-451 (2007) 239-242; Baolong Chen, Cuntao Chang, Zhefeng Zhang, Akihisa Inoue, J. Appl. Phys. 102 (2007) 023515
[5]. D. Turnbull, Under what conditions can a glass be formed?, Contemp. Phys. 10, (1969) 473
[6] Z.P. Lu and C.T. Liu, Acta Mater. 50 (2002) 3501
[7] F.R. de Boer, R. Boom, W.C.M. Mattens, A.R. Miedma and A.K. Niessen. In: F.R. de Boer , D.G. Pettifor, editors. Cohesion in Metals. Amsterdam: The North-Holland Physics Publishing; 1988.
[8] M. Stoica, R. Li, A.R.Yavari, G. Vaughan, J. Eckert, N. van Steenberge, D. Ruiz Romera, J. Alloys Compounds 504S (2010) S123-128
[9] G. Herzer, IEEE Trans. Magn. 25 (1989) 3327-3329.

2. Study of the nanocrystallization kinetics under non-isothermal conditions.

This section corresponds to the Goal 3 of the original project presented in the application for the grant.

Metallic glasses are systems with a disordered structure similar to those in liquids. For this reason the classical treatment of the nucleation and growth phenomena and the crystallisation kinetic models generally applied to liquid-solid phase transformations may also be valid in this kind of systems. Beyond the existing models, the best description of kinetics of phase transformation is given by the so-called Kolmogorov-Johnson-Mehl-Avrami (KJMA) theory [1-5]. This model allows calculating the evolution of the transformed volume along the transformation. Basically a phase transformation proceeds through two different process nucleation of the new phase in the parent one and growth of these nuclei. Both phenomena are described in the Classical Nucleation Theory [6] by models that depend on fundamental thermodynamic quantities such as Gibbs free energy difference between the two phases, viscosity of the melt and interfacial energy between both phases, all of them temperature dependent [7-9]. However, satisfactory results in describing the phase transformation can also be obtained using simpler approximations as a constant activation energy model, where the energy to overcome the potential barrier for nucleation and growth is considered independent of temperature [10-13]. The crystallization mode in metallic glasses is in general a primary crystallization of a new phase with a composition that differs from the parent phase. However, it has been shown that the existing models for polymorphic transformations can be also used in describing the primary crystallization [14]. The knowledge of the kinetics of crystallization of metallic glasses is a key point in order to design controlled procedures for the improvement of the properties that depend on the microstructure such as magnetism. However, from the basic research point of view, it helps to validate the proposed models for phase transformations.
Following the Goal 3 of the project I analyse the crystallization kinetics of non-isothermal transformation curves obtained from calorimetric measurements using the master Curve method grounded in the KJMA framework and we applied it to the study of the transformation mechanisms of three different amorphous metallic alloys. These alloys are $[(Fe_{60}Co_{40})_{0.75}Si_{0.05}B_{0.20}]_{95}Nb_4Zr_1$ (one of the alloys presented in the previous section), $Cu_{47}Ti_{33}Zr_{11}Ni_8Si_1$ and $Fe_{77}Nb_7B_{15}Cu_1$.

In order to study the primary crystallization kinetics alloys, DSC scans for continuous heating rates (β) from 5 to 40 K/min have been performed. The DSC continuous heating curves shows a primary crystallization peak superposed with a significant heat capacity change ΔC_p during the transformation: the heat capacity of the sample shifts gradually from the heat capacity of the undercooled melt to the heat capacity of the nanostructured material [15]. Mathematically the superposition of these two contributions is expressed by:

$$\frac{dQ}{dt} = \frac{d\Delta H}{dt} + \frac{\Delta C_p dT}{dt} x = \Delta H \frac{dx}{dt} - \beta \Delta C_p x \qquad (2)$$

with x the primary transformed fraction. These two contributions to the signal were separated using an iterative procedure, considering that the overall specific heat of the specimen is given by the linear interpolation of the specific heats of the undercooled melt and the crystalline compound [15]. The pure dx/dt signal can be used now to study the transformation kinetics. In the framework of the Kolmogorov-Johnson-Mehl-Avrami the curves can be analysed using the Master Curve method (MCM) introduced by Jacovkis [16,17]. The principles and description of this method is found in that references.
Basically, a set of DSC curves at different heating rates are transformed to curves with the same equivalent heating rate β_{eq}, for each value of the activation energy. Following an iterative procedure for a range of values of the activation energy described in [17], the differences between them are minimized and the optimal value of E_a which leads to the best overlap of the transformed curves can be found. Then, the master curve is an average curve of all the converted curves that contains the kinetic information. The main advantage of this method over the Kisinger's one is that works over all the points of the curve while the other only takes one point into account (the maximum of the curve) and thus, reduces the uncertainity. Also, the experimental $P(x)$ function is obtained. In the case of non-constant Avrami exponent transformations, n is determined locally by fitting the experimental kinetic function by the Avrami kinetic model (eq. 2) in a certain range of x.

$$P(x) = \frac{P_0\left[-\ln(1-x)\right]^{\frac{1-n}{n}}}{n(1-x)} \quad (3)$$

The analysis of the calorimetric curves leaded to following results. In the case of $[(Fe_{60}Co_{40})_{0.75}Si_{0.05}B_{0.20}]_{95}Nb_4Zr_1$ alloy, after applying the MCM method the curves are transformed to the equivalent heating rate of 10 K/min and the master curve is obtained. The apparent activation energy was determined with the best overlapping of the experimental data in the master curve and its value is E_a=494 kJ/mol. This value is similar to those obtained by Li [18] in $[(Fe,Co)_{0.75}Si_{0.05}B_{0.20}]_{94}Nb_6$ E_a=469 kJ/mol. Such a high values are normally associated with transformation process where homogeneous nucleation play an important role. The experimental kinetic curve is fitted in the first stages of crystallization, that is 2%<x<10%, obtaining a value of the Avrami exponent n=2.57 and P_0^{-1} =4.24·10^{27} s. Values of n=2.5 can be interpreted as a transformation that starts through homogeneous nucleation and diffusion-controlled growth. A high value of activation energy, like that we found, is commonly related with homogeneous nucleation mechanism [19]. It is worth noting that in the beginning of the transformation the nuclei are small and well separated so it is reasonable to consider that the Avrami´s conditions of random nucleation and no change in the composition of the matrix are fulfilled. As the transformation proceeds the remnant amorphous matrix is enriched from the atoms expelled from the growing crystals slowing down the transformation until is hindered due to the soft impingement effect as previously observed in primary crystallization transformations in similar metallic glasses [19]. However some microstructural investigations are still pending to support this interpretation.

For the $Cu_{47}Ti_{33}Zr_{11}Ni_8Si_1$ alloy, the curves are transformed to the equivalent heating rate of 20 K/min as shown in figure 5. The best overlap was obtained for an activation energy of E_a = 3.8 eV comparable with the values obtained using other methods E_a = 3.5 eV with Kissinger and E_a = 3.7 eV with isothermal methods [20]. The corresponding kinetic experimental function is plotted in figure 5. The fitting with the Avrami kinetic function in the range of 2 < x < 8 % leads to a value of the Avrami exponent of n = 3.2 and P_0 = 4.68·10^{-23} s. Different interpretations could arise from this value. A first possibility would suggest a 3D interface-controlled growth of quenched-in nuclei. However, this option may be refuted by the TEM microstructural investigations. A more reasonable interpretation suggests a transformation controlled by a nucleation and diffusion-controlled growth mechanism. In this case the n_I > 1 which correspond to an increasing nucleation frequency.

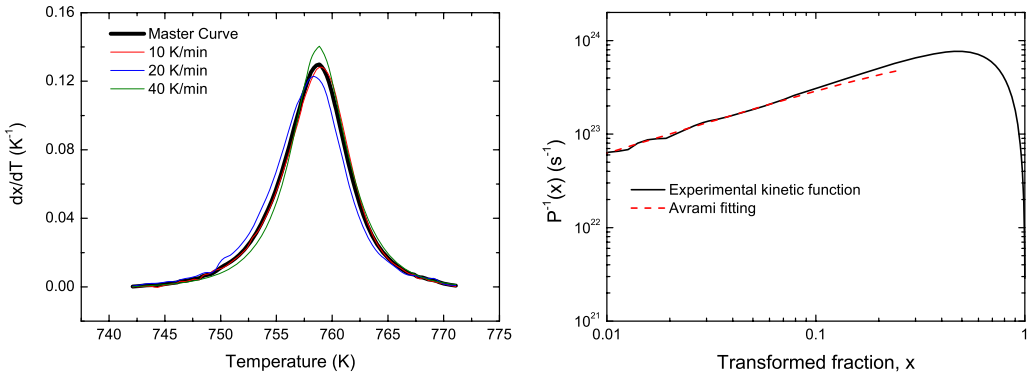

Figure 5. Left: Master Curve and transformed continuos heating curves. Right: Experimental kinetic function and Avrami fitting.

In this case ribbons of $Fe_{77}Nb_7B_{15}Cu_1$, calorimetric curves recorded at different heating rates are transformed using the Master Curve method to an equivalent heating rate of 10 K/min. The value of activation energy that leads an optimum overlap of the transformed curves is E_a = 5.7 eV. This value is typical for this kind of alloys and has been also found in other Fe(Co)NbBCu alloys [21]. The Avrami kinetic function fitting in the first stages (x < 10%) of the experimental curve gives an Avrami exponent $n = 0.8$ and $P_0 = 1.42 \cdot 10^{-34}$ s. This abnormal low value of n at the beginning of the transformation is difficult to interpret by the KJMA model. In order to explain the transformation mechanisms microstructural information is required. The TEM micrographs obtained after heating up to different crystallization stages indicate that nucleation is present over the entire process showing a slight decrease with temperature and nanocrystals with a final size of about 4-6 nm. In this case, the determination of the Avrami exponent with the fitting of constant n Avrami kinetic function is not able to explain the observed microstructure. A simple mathematical model has been proposed to explain the observed microstructure.

Output of the research results.

The results obtained in this section leaded to two publications in peer reviewd journals:

J. Torrens-Serra, I. Peral, J. Rodriguez-Viejo, M. T. Clavaguera-Mora, Microstructure evolution and grain size distribution in nanocrystalline FeNbBCu from synchrotron XRD and TEM analysis, *Journal Non-Crystalline Solids* 358 (2012) 107-113.

J. Torrens-Serra , S. Venkataraman , M. Stoica, U. Kuehn, S. Roth, J. Eckert, Non-isothermal kinetic analysis of the crystallization of metallic glasses using the Master Curve method, *Materials,* 4 (2011) 2231-2243.
.

The results may be presented in international conferences during 2012 such as IWNCS 2012 or ISMANAM 2012.

References

[1] M. Avrami, Kinetics of phase change. I. General theory, J. Chem. Phys. 7 (1939) 1103-1112.
[2] M. Avrami, Kinetics of phase change. II. Transformation–time relations for random distribution of nuclei, J. Chem. Phys. 8 (1940) 212-224
[3] M. Avrami, Granulation, phase change and microstructure. Kinetics of phase change. III, J. Chem. Phys. 9 (1941) 177-184.
[4] W. Johnson, K. Mehl, Reaction kinetics in processes of nucleation and growth, Trans. Am. Inst. Min. Met. Eng. 195 (1939) 416-458.
[5] A. Kolmogorov, Static theory of metals cristallization, Izv. Akad. Nauk SSSR. Ser. Mater. 1 (1937) 355-359.
[6] J. Christian, The theory of transformations in metals and alloys, 2nd Edition,
Materials science and technology, Pergamon Press, 1981.
[7] D. Xu and W. L. Johnson, Crystallization kinetics and glass-forming ability of bulk metallic glasses $Pd_{40}Cu_{30}Ni_{10}P_{20}$ and $Zr_{41.2}Ti_{13.8}Cu_{12.5}Ni_{10}Be_{22.5}$ from classical theory, Phys. Rev. B 74 (2006) 024207 .
[8] D. Turnbull, Under what conditions can a glass be formed?, Contemp. Phys. 10, (1969) 473.
[9] Uhlmann DR. A kinetic treatment of glass formation. J. Non-Cryst. Solids 7 (1972) 337–48.
[10] F. Liu, F. Sommer, C. Bos and E. J. Mittemeijer, Analysis of solid state phase transformation kinetics: models and recipes, International Materials Reviews 25 (2007) 193
[11] A. L. Greer, Crystallisation kinetics of $Fe_{80}B_{20}$ glass, Acta Metall. 30, (1982) 171.
[12] L.A. Perez-Maqueda, J.M. Criado, J. Malek, Combined kinetic analysis for crystallization kinetics of non-crystalline solids, Journal of Non-Crystalline Solids 320 (2003) 84–91
[13] M.C. Weinberg, The use of site saturation and Arrhenius assumptions in the interpretation of non-isothermal DTA/DSC crystallization experiments, Thermochim. Acta 194 (1992) 93.
[14] M. Clavaguera-Mora, N. Clavaguera, D. Crespo, T. Pradell, Crystallisation kinetics and microstructure development in metallic systems, Progr. Mater. Sci. 47 (2002) 559.
[15] N. Clavaguera, M. T. Clavaguera-Mora, and M. Fontana, J.Mater. Res. 13(1998) 744.

[16] D. Jacovkis, Y. Xiao, J. Rodriguez-Viejo, M. Clavaguera-Mora, N. Clavaguera, Mechanisms driving primary crystallization of $Al_{87}Ni_7Cu_3Nd_3$ amorphous alloy, Acta Mater. 52 (2004) 2819.
[17] D. Jacovkis, J. Rodriguez-Viejo, M. Clavaguera-Mora, Isokinetic analysis of nanocrystallization in an Al–Nd–Ni amorphous alloy, J. Phys.: Condens. Matter. 17 (2005) 4897.
[18] R. Li, S. Kumar, M. Stoica, S. Roth, J. Eckert, J. Phys. D: Appl. Phys. 42 (2009) 085006.
[19] J. Torrens-Serra, J. Rodriguez-Viejo, M. T. Clavaguera-Mora, Nanocrystallization kinetics and glass forming ability of the Fe65Nb10B25 metallic alloy, Phys. Rev. B 76 (2007) 214111.
[20] S. Venkataraman, H. Hermann, C. Mickel, L. Schultz, D. J. Sordelet, and J. Eckert, Calorimetric study of the crystallization kinetics of $Cu_{47}Ti_{33}Zr_{11}Ni_8Si_1$ metallic glass, Phys. Rev. B 75, (2007) 104206.
[21] J. Torrens-Serra, P Bruna, J. Rodriguez-Viejo, S. Roth, M. T. Clavaguera-Mora, Effect of minor Co additions on the crystallization and magnetic properties of Fe(Co)NbBCu alloys, Journal of Alloys and Compounds 496 (2010) 202–207.

3. Low-temperature magnetic properties and magnetocaloric effect in Fe-based bulk metallic glasses.

This section corresponds partially to the Goal 4 of the original project presented in the application for the grant.

Recently it has been found a new family of Fe-based metallic glasses with very high glass forming ability and excellent mechanical properties that have been designed by the name of amorphous steels [1]. These alloys are not ferromagnetic at room temperature due to a lower content of Fe than the previous ones. Although, they are not able to be used as soft magnetic materials, the might be interesting as magnetocaloric materials for refrigeration near room temperature and are excellent materials to study magnetoelastic coupling in metallic glasses. The first step was to study the temperature dependence of $Fe_{65-x}Cr_xMo_{14}C_{15}B_6$ alloys with (x=0,2,4). The Curie temperature changes with the composition of the alloy from 156 K for x=4 to 320 K for x=0.
The magnetocaloric effect for the x=0 alloy has been evaluated by the magnetic entropy change using the Maxwell relation [2]. M(H) curves at different temperatures around Curie temperature have been obtained using a QD Squid up to 2 T. The results show a maximum magnetic entropy change of 1.1 J/Kkg. This values is in the same order of magnitude as in other Fe-based metallic glasses with the advantage of a near room-temperature maximum. Further evaluation and investigation still running. The magnetomechanical properties are currently analysed in collaboration with the Grup de Física de Materials of the Universitat de les Illes Balears. The low temperature magnetomechanical coupling has been analysed by mechanical spectroscopy using ultrasonic frequencies. The experimental setup can be found in Ref [3]. The preliminary results obtained show a pure magnetoelastic contribution at Below Curie temperature. Also, some anomalies are observed at about 40 K. This research will be continued in the following years dure to the high interesting results obtained in the first experiments.

Output of the research results.

The results obtained will be published in high impact journals in the next years and may be presented in international conferences.

References

[1] V. Ponnambalam, S.J. Poon, and G.J. Shiflet, Fe-based bulk metallic glasses with diameter thickness larger than one centimeter. J. Mater. Res. 19, 1320 (2004).
[2] S.-G. Min, Kyeong-Sup Kima, Seong-Cho Yu, Kyu-Won Leeet, Materials Science and Engineering A 449–451 (2007) 423–425.
[3] M.L. Corró, S. Kustov, E. Cesari, Y.I. Chumlyakov, Magnetomechanical damping in Ni–Fe–Ga poly and single crystals , Materials Science and Engineering: A, 521-522, 2009, 201-204